energies

MDPI

Article

SolNet: A Convolutional Neural Network for Detecting Dust on Solar Panels

Md Saif Hassan Onim [1,†], Zubayar Mahatab Md Sakif [2,†], Adil Ahnaf [1,†], Ahsan Kabir [1,†], Abul Kalam Azad [3,*,†], Amanullah Maung Than Oo [4,†], Rafina Afreen [2,†], Sumaita Tanjim Hridy [2,†], Mahtab Hossain [2,†], Taskeed Jabid [2,†] and Md Sawkat Ali [2,*,†]

[1] Department of Electrical, Electronic and Communication Engineering, Military Institute of Science and Technology, Mirpur Cantonment, Dhaka 1216, Bangladesh
[2] Department of Computer Science and Engineering, East West University, Dhaka 1212, Bangladesh
[3] School of Engineering and Technology, Central Queensland University, 120 Spencer Street, Melbourne, VIC 3000, Australia
[4] School of Engineering, Computer and Mathematical Sciences, Auckland University of Technology, Auckland 1010, New Zealand
* Correspondence: a.k.azad@cqu.edu.au (A.K.A.); alim@ewubd.edu (M.S.A.); Tel.: +61-396160409 (A.K.A.)
† These authors contributed equally to this work.

Abstract: Electricity production from photovoltaic (PV) systems has accelerated in the last few decades. Numerous environmental factors, particularly the buildup of dust on PV panels have resulted in a significant loss in PV energy output. To detect the dust and thus reduce power loss, several techniques are being researched, including thermal imaging, image processing, sensors, cameras with IoT, machine learning, and deep learning. In this study, a new dataset of images of dusty and clean panels is introduced and applied to the current state-of-the-art (SOTA) classification algorithms. Afterward, a new convolutional neural network (CNN) architecture, SolNet, is proposed that deals specifically with the detection of solar panel dust accumulation. The performance and results of the proposed SolNet and other SOTA algorithms are compared to validate its efficiency and outcomes where SolNet shows a higher accuracy level of 98.2%. Hence, both the dataset and SolNet can be used as benchmarks for future research endeavors. Furthermore, the classes of the dataset can also be expanded for multiclass classification. At the same time, the SolNet model can be fine-tuned by tweaking the hyperparameters for further improvements.

Keywords: CNN; SolNet; classification; deep learning; image processing; solar panel; PV; dust

check for updates

Citation: Onim, M.S.H.; Sakif, Z.M.M.; Ahnaf, A.; Kabir, A.; Azad, A.K.; Oo, A.M.T.; Afreen, R.; Hridy, S.T.; Hossain, M.; Jabid, T.; et al. SolNet: A Convolutional Neural Network for Detecting Dust on Solar Panel. *Energies* **2023**, *16*, 155. https://doi.org/10.3390/en16010155

Received: 22 November 2022
Revised: 13 December 2022
Accepted: 16 December 2022
Published: 23 December 2022

Copyright: © 2022 by the authors. Licensee MDPI, Basel, Switzerland. This article is an open access article distributed under the terms and conditions of the Creative Commons Attribution (CC BY) license (https://creativecommons.org/licenses/by/4.0/).

1. Introduction

The use of fossil fuels to produce electric power explicitly increases greenhouse gas emissions (GHGs) in the environment. This climate impact can be considerably reduced by utilising renewable resources, particularly producing electricity from solar energy [1]. In 2021, the capacity of global renewable production increased by 257 GW and currently amounted to 3064 GW. Solar energy continued to lead the capacity expansion, with an increase of 133 GW (+19%); hence, the global solar capacity reached 849 GW in 2021. For instance, China had the highest contribution of 307 GW of capacity enhancement from its annual capacity of 253 GW in 2020. On the other hand, the USA expanded its solar capacity up to 27% which amounted to 94 GW of solar generation. Figure 1 shows the enhancement of global solar capacity from 1996 to 2021 of the seven leading countries producing solar energy [2].

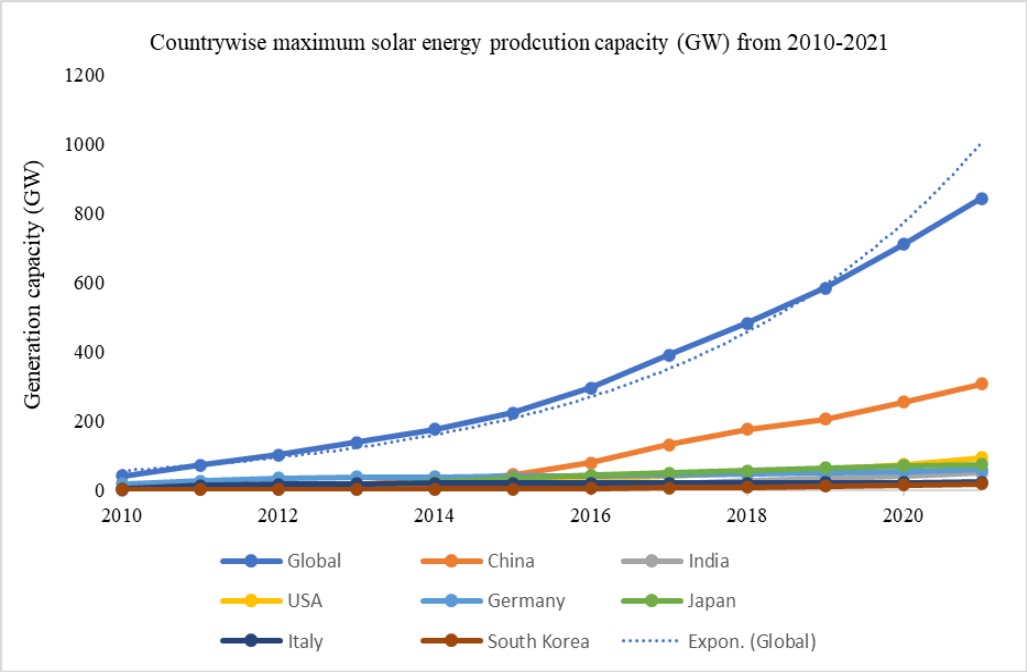

Figure 1. Global solar production for the top seven countries [3].

Photovoltaic (PV) cells are one of the promising solar technologies, directly converting sun radiation into electricity at 15% to 20% nominal efficiency. However, the current rate of global solar expansion is impacted by this poor efficiency, and the maximum utilisation depends on multiple environmental factors such as operating temperature, wind velocity, shading loss, hail, snow, air density, sky condition, and dust on the PV surface. Among all these, dust, dirt, and other particles cause soiling losses, which reduce the performance of PV modules [4]. Dust refers to any particle found in the environment that is less than 10 mm in diameter and generated from many sources such as sand, soil, rocks, contraction debris, volcanic smoke vapor, eroded limestone, and bird droppings [5]. The dust particles stored in the panels can exacerbate the soiling effect and regularly reduce the overall generation. The deposition of dust particles is influenced mainly by the sun's angle of inclination and the material of the PV module's cover in addition to the dust buildup, ambient temperature , tilting angle, soil conditions, and plants in the area. Dust accumulates on the PV surface in three ways: occult deposits (mist, cloud, high humidity, moisture in fog, dew), dry deposits (wind), and wet deposits (rainfall). Depending on the local environmental factors, the dust's chemical and mineral makeup varies. Due to the fact that the placement of PV installations also impacts dust buildup, the deposit rate is higher close to factories, volcanic regions, and regions vulnerable to sandstorms [6].

The performance and efficiency of the PV modules differ depending on dust accumulation in the surrounding environment of PV installation. For example, during poor irradiation conditions, dust particles' size is larger and more significant; hence, the wavelength of the radiation is scattered. The PV panel output falls when the dense coating of dust on the module surface change the optical properties, such as raising light reflection, decreasing transmissivity, and leading to electrical power loss. Moreover, dust causes a temperature variation, resulting in a slight difference in short-circuit current and a decrease of voltage in open circuit, both decreased by 15 to 20% and 2 to 6%, respectively [7]. In another study, the dust effect of different PV modules showed that 33% of output power was reduced with a dust density of 4.25 mg/cm^2 in a-Si and CdTe type modules [8]. It has been also observed that dirty Si solar cells had a reduced efficiency of 66% over a period of six months. On the other hand, 8.41% less power was generated from a dusty module in comparison with a clean one [9].

Numerous research studies examining the impact of deposited dust on PV panels revealed that tropical climatic conditions, particularly in Asia, are where soiling rates are highest. According to a study on the dust effect conducted in India, between 20% and 25% of the PV-generated energy may be lost in the process. [10]. According to an experimental study conducted in Lahore, Pakistan, a PV panel can lose between 10% and 40% of its output power due to the rise in surface temperature and dust levels [11]. Another study in Nepal showed that a solar module's performance decreased by 29.76% because of natural dust accumulation despite the module being cleaned regularly for five months [12]. Experiments conducted in China showed that the efficiency of modules ranges from 0% to 26% when the dust density rises to 22 g/m^2 [13]. In Southeast Asian, the peak power from PV was reduced by 18% due to dust in a study in Malaysia [14], whereas the dust accumulation on the PV panel decreased power by 10.8% with a mean relative humidity of approximately 52.24% in an experiment in Indonesia [15]. According to studies in the Middle East, maximum output power decreased by 34% [8] in Kuwait, whereas an experiment in Saudi Arabia showed that the output of PV modules might decrease by 26% to 40% [16]. A study conducted in Iran showed that a lack of rain for 70 days causes 6.0986 (g/m^2) of dust to accumulate on the surface and reduce output power by 21.47%, which is a 289-kWh energy reduction in provided energy for each 78 4.845 kW PV system [17]. Additionally, six different places in northern Oman were used to gather natural dust for a study, and its characteristics were studied. It revealed that if a PV module is not cleaned for three months, soiling loss causes a 35–40% reduction in power output [18]. However, it is clearly observed that the factors are varied at different locations according to the types of dust, and the impact on PV cells is inevitable. Therefore, it is highly important to clean the panels at regular intervals to maximise PV generation. To ensure clean panels, the detection of dust is a prime need.

To detect the amount of dust on the panels, multi-dimensional approaches such as thermal imaging, image processing, sensors, cameras with IoT, machine learning, and, deep learning are used. Out of these methods, in the thermal imaging detection method a thermal image scanner or an infrared camera detects or captures the infrared energy of objects since infrared light and heat are not visible to human eyes. A thermal camera takes infrared pictures showing heat emitted from an object or material at temperatures above zero degrees and sends a message to the appropriate command center [19]. Such a technique was used by Phoolwani et al. [20] to detect the change in performance of PV panels in both favorable and unfavorable circumstances. The researchers also observed V_{max}, P_{max} and $fill\ factor$ through the PV analyser, and the thermal image was used to pinpoint the PV locations that needed to be cleaned. Cubukcu et al. [21] worked with 19 separate PVPSs in Turkey to detect defects using thermal imaging which performed better in terms of effectiveness and efficiency than other available methods.

IN contrast, IoT and sensor-based techniques are used for both detection and periodic cleaning of the panels. A prototype was proposed by Thomas et al. [22] where a wet cleaning process was introduced, and this method saved the surface from being scratched and resulted in an energy-efficient cleaning system. In another study, Zainuddin et al. [23] introduced a live monitoring method for solar cells with the help of IoT, and a smartphone app was used to monitor the electricity produced and clean the PV surface as needed. Related research was conducted by Mohammed et al. [24] that employed Arduino with a dust sensor (DSM501A) which is low-cost and smaller than other systems for both detection and automatic cleaning system. Experimental performance analysis showed that the robot involvement in the solar panel improved the system's overall efficiency in the work of Kumar et al. [25]. Recently, satellite remote sensing has been widely used in various sectors, such as solar panel dust or sand detection, geolocation, soil quality monitoring, rice paddy status, etc. as shown by Minh et al. [26]. Such an approach is used by Google Earth Engine (GEE) with the Dry Bare Soil Index (DBSI) method that showed a detection accuracy of 89.6% as found by Supe et al. [27].

Digital image processing is another prevalent method of detecting dust. In terms of image processing, there is no physical connection between the solar panel and the camera. For instance, Abuqaaud et al. [28] presented a novel approach for dust detection using image processing with computer vision. In this method, hue layer was used to extract features from HSV colour with a co-occurrence gray level matrix, and finally sort clean and dirty panels using a linear method of classification. For further development in the detection of dust, two methods, namely digital and infrared cameras, were used by Tribak et al. [29]. By using techniques such as linear regression, spectral decomposition of light, and other image processing techniques, dust can be detected on the exterior of PV modules with an accuracy of 90%. The researchers also proposed another image processing method where they formed a correspondence curve among the telltale image entropy and the generated power. The experiment was conducted with different concentrations of dust, where it was found that power production was nearly zero with the panels 100% covered with dust. Aside from the advantages of available techniques for dust detection using thermal imaging and IoT, it has some drawbacks. For instance, the IoT system must be connected to a sensor whose efficiency can depreciate with time. Furthermore, thermal imaging needs a very high-quality camera and sophisticated software to produce correct results. Both processes are high maintenance and costly. Moreover, image processing systems have a low accuracy rate of detection. Furthermore, the dust types are not identical in all the places on Earth. The systems need to be tangible, which is difficult for IoT and thermal imaging detection systems.

The recent development of artificial intelligence (AI)-based dust detection methods has introduced a new perspective and is becoming more popular [30]. Different approaches, such as the measurement of the dimensions of dust particles using computer vision for high-resolution images by Igathinathane et al. [31], identification of particles using random forest by Maitre et al. [32], and k-nearest neighbors (*k*-NN) by Proietti et al. [33], have been used by researchers for the classification and detection of dusty panels. Deep learning models were also used for such classification. With the information gathered from pictures of dust on solar panels, Saquib et al. [34] created an artificial neural network (ANN), and the output was preserved in the form of voltage and current. Other parameters, such as irradiance, current, and voltage, were measured with the help of LDR and multi-meter. The developed neural network had only one hidden layer with nine neurons. Thus, the output voltage of the panels was forecast with the irradiance and amount of dust as the input. For the same purpose, a convolutional neural network (CNN) method was proposed by Mehta et al. [35]. Using web-supervised learning, the impact area of dust obtained from the predicted localisation masks is classified into soiling types. Bi-directional input-aware fusion (BiDIAF) was used for featuring the data. The accuracy of power loss prediction promised, which is about 3% and localisation about 4%, improved by 226 BiDIAF. In a weakly supervised manner, localisation improved by about 24% in that research. For the prediction of the concentration of uneven dust gathering, a deep residual neural network in conjunction with image processing and cleaning methods was used by Fan et al. [36], where they achieved R2 and mean absolute error (MAE) of 78.7% and 3.67%. In another study, 30,000 images were taken with binary labeling, and the power loss was calculated keeping the same irradiance level. The CNN LeNet model was employed with custom layers of dropouts and pooling, where Maity et al. [37] achieved an accuracy of 80% with the mean squared error of 0.0122. Deep CNN architectures were been applied by Zyout et al. [38] to build a model using a dataset of 599 images. The dataset was applied to AlexNet, LeNet, and VGG-16 models where AlexNet achieved an accuracy of 93.3%. A study was conducted on PV degradation and irregularity patterns using reviewed different machine and deep learning methods using computation period, characterization techniques, dataset, and feature extraction mechanisms [39]. In another study, a deep belief network was developed to detect the dust on PV panels, and the proposed model achieved higher accuracy in comparison with other machine-learning-based models [40]. Another study considered the integration of Mobile-Net and VGG-16 CNN techniques for the evaluation of solar

panels, combined with the physical lotus effect methodology that allows for solar panel maintenance [41]. Similar to this, for a PV performance study, the effectiveness of various machine learning algorithms, including auto-encoder long short-term memory (AE-LSTM), Facebook-prophet, and isolation forest, was evaluated. The results offer clear insights to assist in making an informed decision [42]. In further study, researchers kept six PV modules in Sohar city, Oman, where a deep-learning-based modular neural network was used to investigate the impacts of dust and temperature on PV power production [43].

However, the world has envisioned notable changes with multiple applications of neural networks where the models can learn to predict by themselves. Such models can be trained with any local dataset according to the region where the panels are set up. Thus, a new possibility for the improvement of dust detection through research emerges. However, for building such models, a vast dataset is needed. Unfortunately, such datasets are not publicly available for solar panel dust analysis to the best of the author's knowledge. The scarcity of good and balanced datasets makes it difficult to make a model with appropriate parameters, and a distinct research gap for assessing state-of-the-art algorithms with appropriate datasets exists. In this paper, a new dataset of dusty and clean panels is introduced which is free from class imbalance. Applying the current state-of-the-art (SOTA) algorithms, this new dataset has accuracy of nearly 100% on test sets. Then, a new CNN architecture named SolNet, which deals specifically with dust detection on PV panels, is proposed. Thereafter, the performance of the proposed SolNet and other SOTA is compared to validate its efficiency, and outcomes are discussed. Finally, both dataset and SolNet are proposed for benchmarking for future research.

The following provides a summary of the contributions in this article:

- A new dataset of the dusty and clean solar panel is introduced that is free from class imbalance.
- The current state-of-the-art (SOTA) algorithms are performed nearly 100% accurately on test sets of our dataset.
- SolNet, a CNN architecture that deals specifically with dust detection on solar panels is proposed and tested.
- The proposed model is evaluated and compared with SOTA to validate its efficiency.
- Both datasets and SolNet are proposed as benchmarks for future research endeavors.

This article has been arranged into several sections. In Section 2, the CNN-based dust detection methods are discussed. The following Section 3 illustrates the experimental setup with the necessary specifications. Results analysis and discussion are discussed in Sections 4 and 5. Finally, Section 6 contains the concluding remarks and future works about the research.

2. Methodology

This section of the paper describes the data analysis process and development of the CNN-based "SolNet" model for dust detection that achieves the aim of this study. The first part appraises and evaluates our proposed dataset. For that purpose, the dataset was prepared per the method mentioned in Section 2.1. Afterward, the dataset is used to train in each of the prominent object detection models, such as VGG16 [44], InceptionV3 [45], Resnet50 [46], and AlexNet [47]. After the training, the generated weights act as pre-trained models for the test set. The performance is evaluated in Section 4 based on the prediction accuracy of the test set. The full workflow is presented visually in Figure 2. Secondly, analysis and evaluation of the performance of our proposed SolNet is conducted in terms of the evaluation metrics selected such as accuracy, loss, and complexity of the model. The same dataset with 5-fold cross validation is used to find the average accuracy and the fold with the highest accuracy.

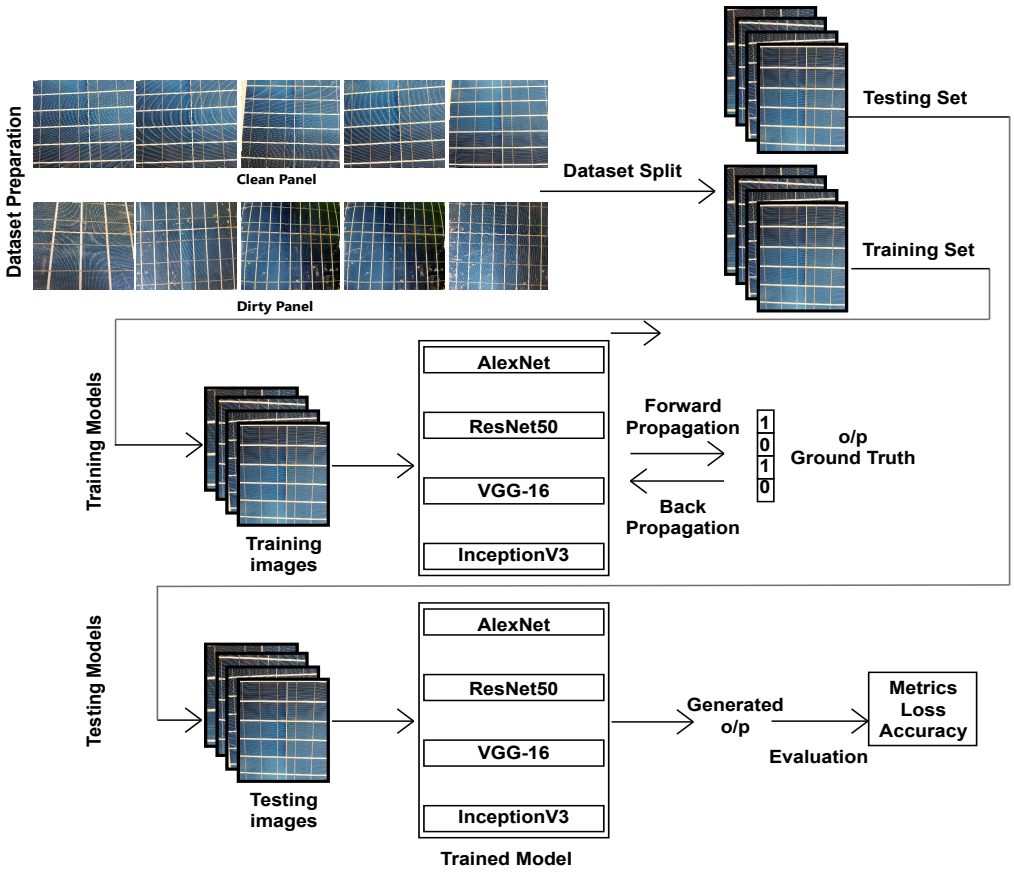

Figure 2. Workflow of our work.

The next part of the section first presents data collection and construction of the proposed dataset. Then, we briefly introduce the current state-of-the-art CNNs for object and pattern recognition and architectures followed by a discussion of the overall workflow. Finally, the proposed method with the architecture of SolNet and its algorithm is explained.

2.1. Dataset Description

Images for the dataset were collected from various regions in Bangladesh. This ensured different levels of dust on the panels. The initial classification was decided to be *clean* and *dirty*. After data curating, 2231 images were finalised for the test and train set with 1130 images of *clean* class and 1101 images of *dirty* class. Each image was labelled manually for the classes for supervised learning. According to the division of the dataset, the training set and the test set distribution is demonstrated in Table 1. Although image shapes in the dataset are 3-channel square-shaped of $227 \times 227 \times 3$, the initial captured images were taken at a random shape to keep all the features intact. The final version of the dataset has squared-shaped images that can be fed to any neural network after reshaping. This made it possible for our dataset to be tested on models with varying input shapes. Some labelled images from the dataset are shown in Figure 3.

Table 1. Train–Test split of dataset.

Image Split	Clean Panel	Dirty Panel
Training Images	708	683
Testing Images	422	418
Total Images	1130	1101

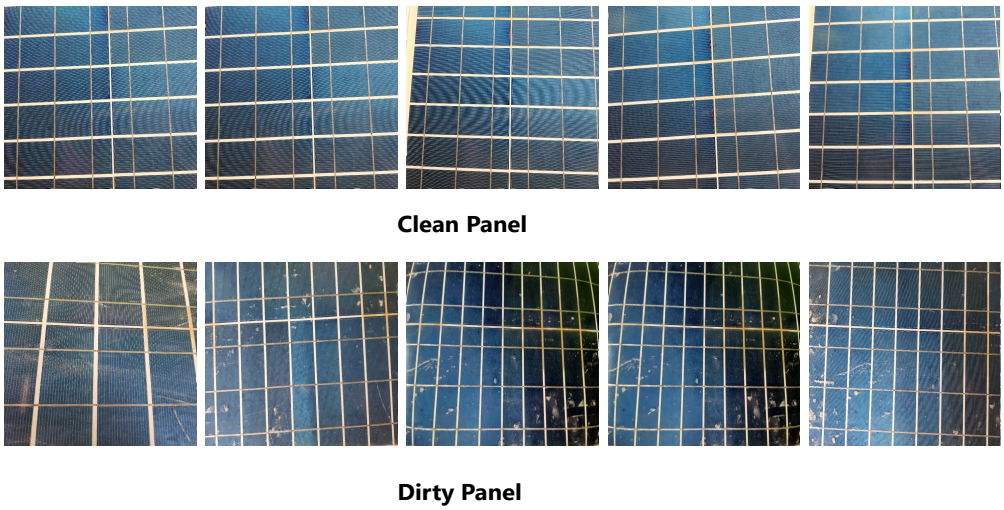

Figure 3. Clean and dirty solar panel images from dataset.

2.2. AlexNet

Proposed by Simonyan et al. [47], AlexNet contains 5 convolutional layers in addition to 3 fully connected layers with 60 million parameters. Its architecture has a pattern of the convolutional layer followed by another convolutional layer. It utilises *relu* for the activation functions in hidden layers and *Softmax* for its output layer. The architecture of AlexNet is shown in Figure 4, and details of each layer are shown in Table 2 .

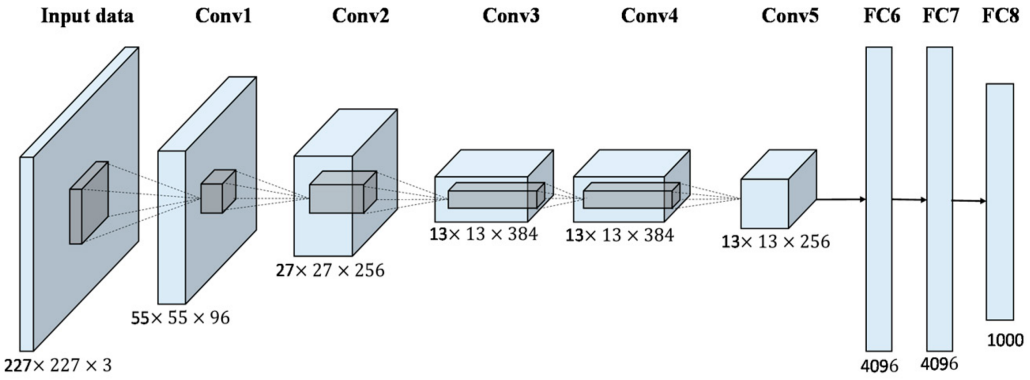

Figure 4. Architecture of the AlexNet model.

Table 2. AlexNet layers.

Layer Name	Input Shape
Conv1	55 × 55 × 96
Pooling	27 × 27 × 96
Conv2	27 × 27 × 256
Pooling	13 × 13 × 256
Conv3	13 × 13 × 384
Conv4	13 × 13 × 384
Conv5	13 × 13 × 256
Pooling	6 × 6 × 256
Fully Connected 1	4096
Dropout	4096
Fully Connected 2	4096
Fully Connected 3	1000

2.3. Resnet50

A residual neural network(ResNet) proposed by He et al. [46] is an artificial neural network that works by jumping over some layers (double or triple layers) that contain non-linearity and batch normalisation by utilising shortcuts and skip connections. In the starting training steps, fewer layers use skipping effectively to simplify the network. The 50-layer deep convolutional neural network contains more than 60 million trainable parameters. The default input size is $224 \times 224 \times 3$ for the network. Resnet50's architecture is illustrated in Figure 5 with further details in Table 3.

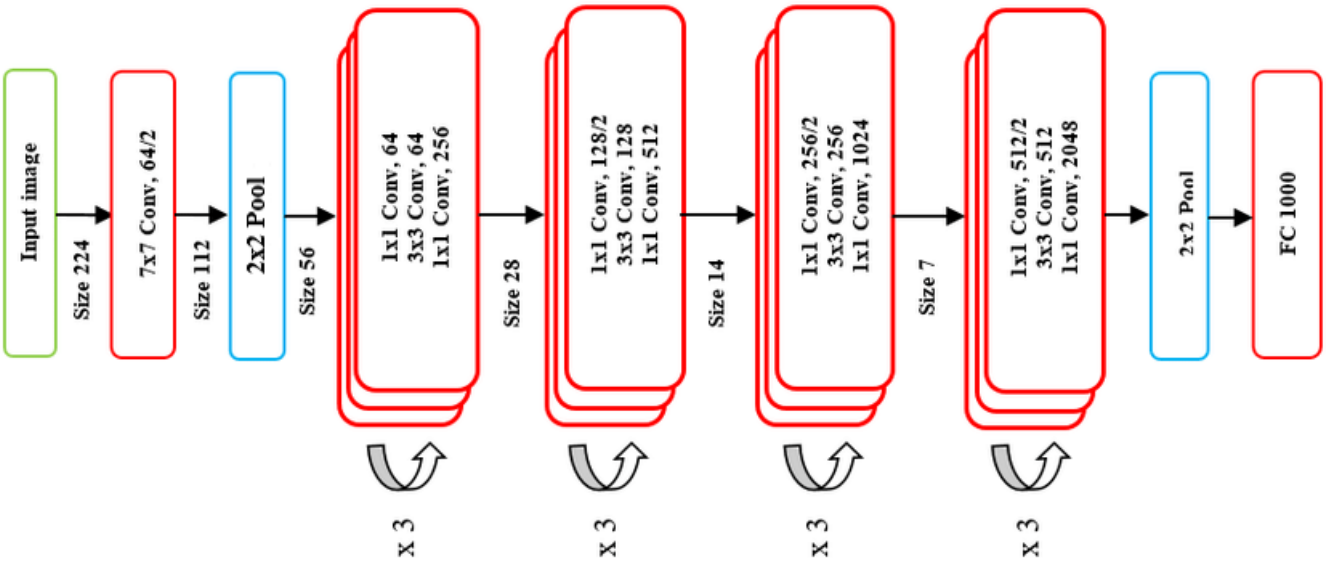

Figure 5. Architecture of Resnet50 model [46].

Table 3. ResNet50 layers.

Layer Name	Input Shape
Conv 1	$112 \times 112 \times 64$
Pooling	$56 \times 56 \times 64$
Conv Block 1	$56 \times 56 \times 256$
Conv Block 2	$28 \times 28 \times 512$
Conv Block 3	$14 \times 14 \times 1024$
Pooling	$7 \times 7 \times 2048$
Fully Connected	1000

2.4. InceptionV3

In ILSVRC2014 [48], Google Net introduced a new CNN called Inception, a multi-level feature extractor. It can compute different types of feature extractions inside the same network module with parallel convolutional layers and separate filter sizes. In the Inception method, all the learned filters are used in the 22-layer architecture. It generates sparse structures that decrease the cost of computations. Its architecture and layer shape are shown in Figure 6 and Table 4, respectively.

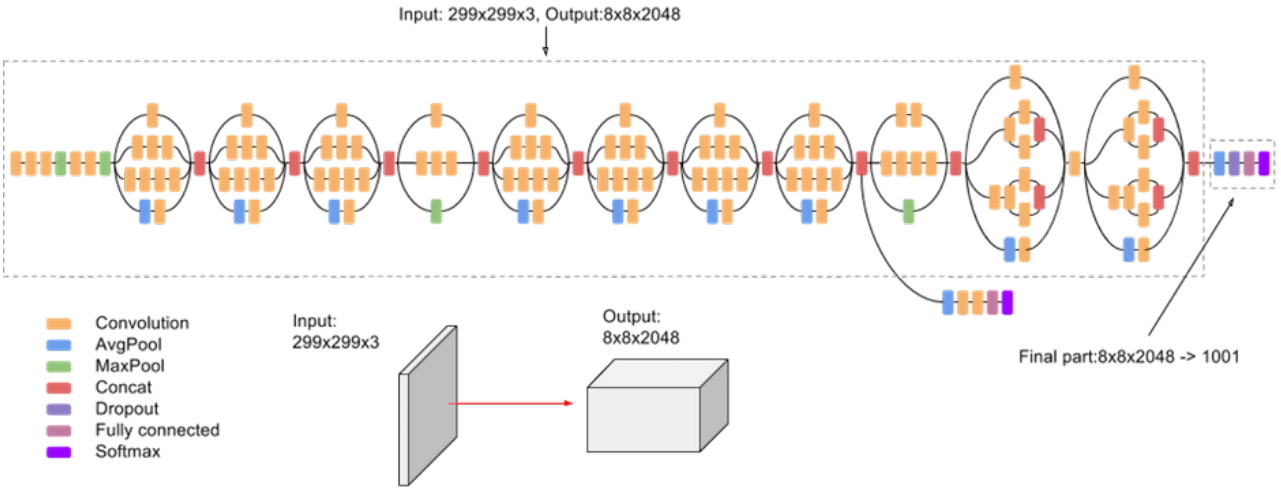

Figure 6. Architecture of InceptionV3 model [48].

Table 4. InceptionV3 layers.

Layer Name	Input Shape
Conv	$299 \times 299 \times 3$
Conv	$149 \times 149 \times 32$
Conv Padded	$147 \times 147 \times 32$
Pooling	$147 \times 147 \times 64$
Conv	$73 \times 73 \times 64$
Conv	$71 \times 71 \times 80$
3× Inception	$35 \times 35 \times 288$
5× Inception	$17 \times 17 \times 768$
2× Inception	$8 \times 8 \times 1280$
Pooling	$8 \times 8 \times 2048$
Linear	$1 \times 1 \times 2048$
Dense	$1 \times 1 \times 1000$

2.5. VGG16

VGG16 is a convolutional neural network model which has been proposed by Simonyan and Zisserman [44] from the University of Oxford and created by the visual geometric group (VGG). The model achieves 92.7% top-5 test accuracy in ImageNet. VGG-16 is a 16-layer neural network model that involves a 3×3 convolutional neural network. It has 138 million parameters. The default image input size is 224×224. Its architecture is shown in Figure 7 and the layer details are given in Table 5.

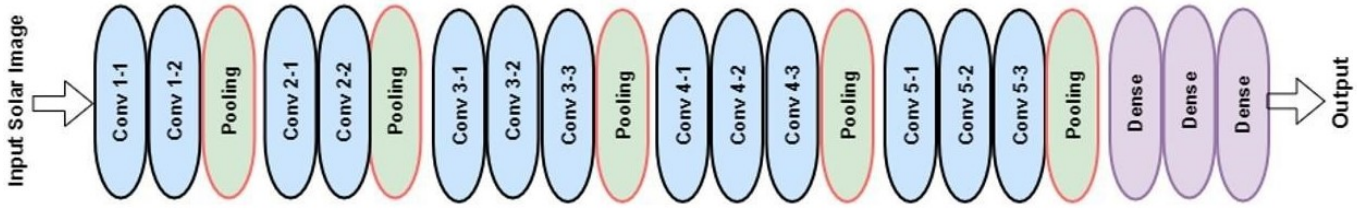

Figure 7. Architecture of VGG16 model [44].

Table 5. VGG16 layers.

Layer Name	Input Shape
Conv 1-1	$224 \times 224 \times 64$
Conv 1-2	$224 \times 224 \times 64$
Pooling	$112 \times 112 \times 64$
Conv 2-1	$112 \times 112 \times 128$
Conv 2-2	$112 \times 112 \times 128$
Pooling	$56 \times 56 \times 128$
Conv 3-1	$56 \times 56 \times 256$
Conv 3-2	$56 \times 56 \times 256$
Conv 3-3	$56 \times 56 \times 256$
Pooling	$28 \times 28 \times 256$
Conv4-1	$28 \times 28 \times 512$
Conv4-2	$28 \times 28 \times 512$
Conv4-3	$28 \times 28 \times 512$
Pooling	$14 \times 14 \times 512$
Conv5-1	$14 \times 14 \times 512$
Conv5-2	$14 \times 14 \times 512$
Conv5-3	$14 \times 14 \times 512$
Pooling	$7 \times 7 \times 512$
Flatten	25088
Dense	4096
Dense	4096
Dense	1000

2.6. Proposed CNN for Dust Detection: SolNet

This study includes a new CNN architecture, SolNet, to classify solar datasets into clean and dirty panels. It consists of 8 *convolutional* and *pooling* layers with 3 *dense* layers also known as *fully connected* layers. This model was built to ensure the reduction of computational complexity with a lower number of trainable parameters. The *max-pooling* layers with *dropouts* were also used to reduce model over-fitting. After the input layer, 2 layers of *conv-pool* pairs are taken. The convolution layer includes 64, 128, and 256 filters with a kernel size of 11×11, 5×5, and 2×2, and the strides are 4×4 and 1×1. After each pair, a *batch normalisation* layer is added which reduces the training epoch drastically for the parallel processing. The *dense* layers are added after the flattened layer. The last *dense* layer, i.e., the *output* layer, has an activation function of *sigmoid*. The proposed SolNet architecture diagram is presented in Figure 8.

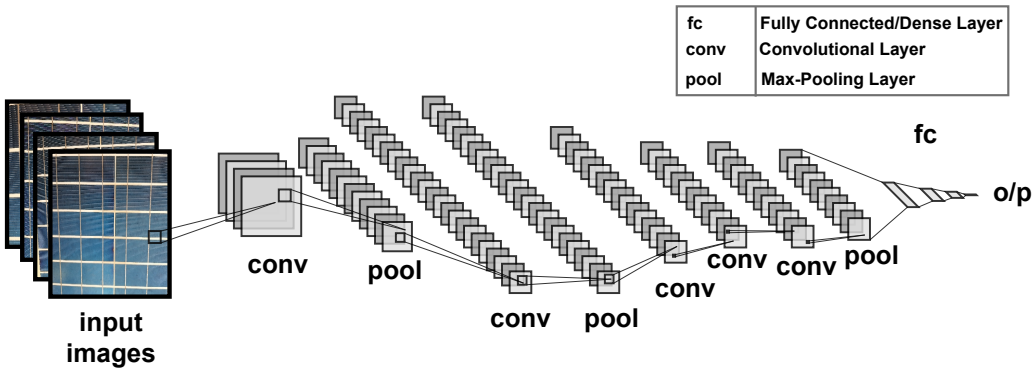

Figure 8. SolNet architecture.

The number of trainable parameters is the key factor in determining the complexity of a model. This includes the total number of neurons that are used to develop the connection between the layers. A dense layer is designed with m and n as input, and output nodes, respectively, will have a total of $(n + 1) \times m$ trainable parameters. The pooling and dropout layers are added to make the training process faster and easier for the algorithm, but these

layers are not trainable. The convolutional layers are built with p and$q$ as input, and output feature maps incorporated with a filter of size $i \times j$ will have total trainable parameters of $(i \times j \times p + 1) \times q$. The calculations give a total of 56 million trainable parameters for our proposed SolNet architecture. The whole workflow for training and testing with SolNet is illustrated in Figure 9.

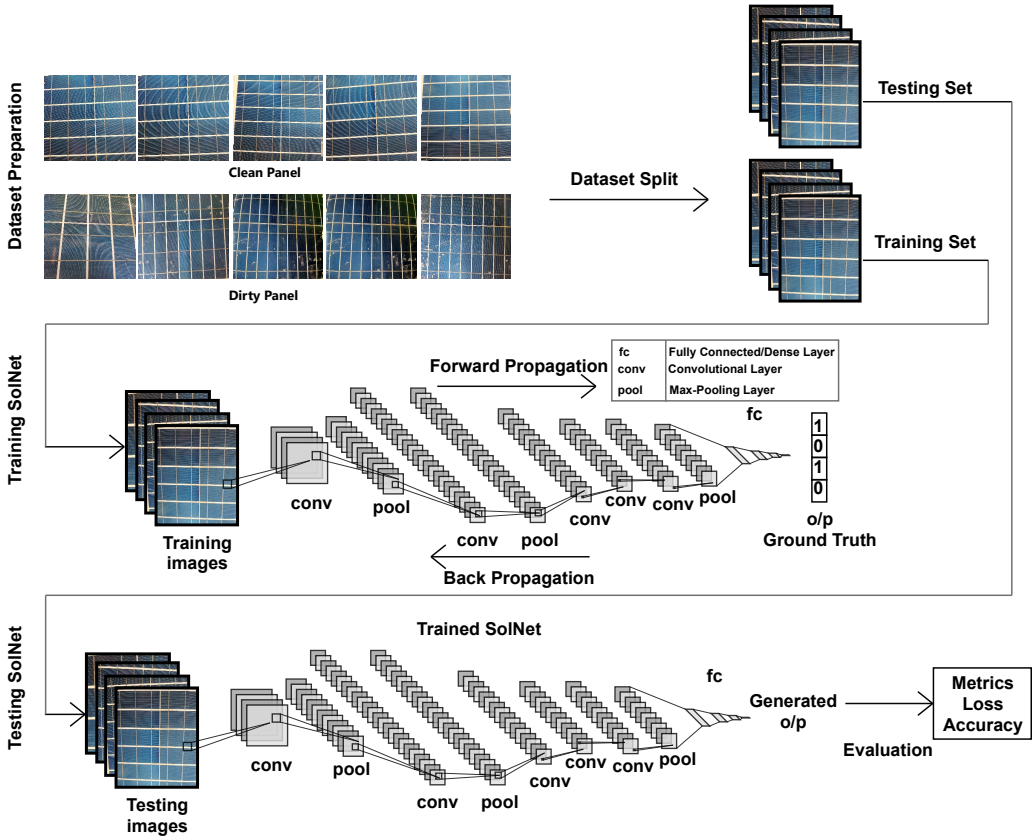

Figure 9. Workflow of proposed method.

3. Experimental Setup and Training

As the problem formulated suggests, it is a binary classification problem. Equation (3) provides the class prediction with output layer activation of *sigmoid* (σ_o) shown in Equation (1), although the hidden layers have activation of *relu* (σ_h) shown in Equation (2). The entropy, i.e., loss to optimise, is chosen to be the *binary cross entropy loss* shown in Equation (4).

$$\sigma_o(z) = \frac{1}{1 + e^{-z}} \tag{1}$$

$$\sigma_h(z) = \max(o, z) \tag{2}$$

$$class = arg_max\left[\sigma\left\{(W_i)^T \times \phi(X_j) + b^i\right\}\right] \tag{3}$$

$$loss = \frac{1}{N}\sum_{i=1}^{N} -\{y_i \times log(P_i) + (1 - y_i) \times log(1 - P_i)\} \tag{4}$$

where W_i, X_j, and b_i are the weight, inputs vector, and bias for ith and jth instances, respectively, N is the total number of samples, y_i is the expected outcome, and P_i is the probability of that outcome.

Training the SolNet requires following Algorithm 1. The sequential development of the CNN algorithm is presented similarly to the work of Onim et al. [49].

Algorithm 1 `train_SolNet`$(\cdot)$

Input: *Dataset*, `SolNet`$(\mathbf{W}, \mathbf{b})$
Output: `trained_SolNet`$(\cdot)$
Initialise:
  $\mathbf{W} =$ `random`$(\cdot)$
  $\mathbf{b} =$ `random`$(\cdot)$
  $Lr = 0.0001$
  $epochs = 30$
$[\mathbf{X}_{train}, \mathbf{X}'_{test}] \leftarrow$ `train_test_split`$(Dataset)$
while $epoch \leq epochs$ **do**
  Perform forward propagation with Equation (3)
  Calculate cost for FP from Equation (4)
  Perform back propagation with gradient descent.
  Optimise cost function with Adam optimiser
  $[\mathbf{W}', \mathbf{b}'] \leftarrow$ `gradient_descent`$(\mathbf{W}, \mathbf{b}, \mathbf{X}_{train}, \mathbf{loss})$
end while
`save`$(trained_SolNet)$

The SolNet is presented as a function of weights and biases that keeps updating during the training process. There are two kinds of input in the algorithm. One is the hyperparameters which are changeable before the training. The other is the input dataset. Finally, after forward and backpropagation, as the error is being optimised, weights in the SolNet are trained. Afterwards, the trained model is saved on a local drive for testing. The implementation can be found at https://github.com/Onimee58/SolNET (accessed on 13 December 2022).

Hyperparameters play a significant role in training a model. Although most of the decisions for hyperparameters are made by trial and error, there are still some conventions used in the current literature that are implemented in the current work. Training hyperparameters for the SolNet are listed in Table 6.

Table 6. Training hyperparameter and hardware.

Parameter	Value
Backbone	Custom
Classes	2(Binary)
Batch size	32
Image size	$227 \times 227 \times 3$
Optimiser	Adam
Learning rate (Lr)	0.0001
Loss	Binary Cross-entropy
Output layer activation	sigmoid
Epochs	30
Processor	Xeon (2.3 GHz)
RAM	12 GB
GPU	Tesla K80 (12 GB)

4. Result Analysis

In this section, the experimental results are presented and analysed. First, the validation of the proposed SolNet was conducted on the test set, and its performance was analysed. Afterwards, the performance was visualised using a confusion matrix. Finally, the results of SolNet were compared with those of SOTA models. The metrics used for the evaluation are *Accuracy* and *Precision*. Equation (5) defines *Accuracy*.

$$Accuracy = \frac{TruePositive + TrueNegative}{TruePositive + FalsePositive + TrueNegative + FalseNegative} \quad (5)$$

Several techniques were used to obtain a mean accuracy on the test set as a performance evaluation of our proposed model. Figure 10 shows the loss and accuracy vs, epochs for each of the five folds used for cross validation. It also shows that the model has been trained for 30 epochs to save the model from over-fitting as the accuracy became nearly constant.

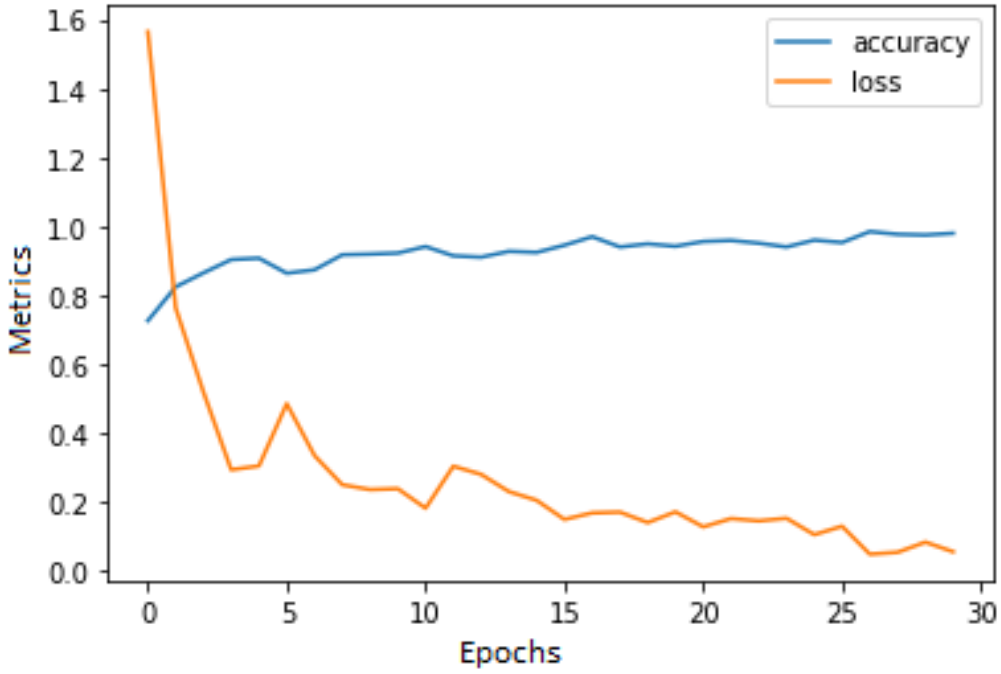

Figure 10. Loss and accuracy vs. epochs during training.

Cross-validation helps to shuffle the input vectors in a way that brings out a model's performance in each fold of the dataset. After five-fold cross validation, the average accuracy of SolNet on our dataset is 98.2% with a maximum of 99.62%. Accuracy on each fold is shown in Table 7.

Table 7. Performance of SolNet for 5-fold Cross validation.

Fold Sequence	Avg Accuracy	Loss
Fold-1	99.62% (highest)	0.89
Fold-2	96.46 (lowest)%	1.29
Fold-3	98.52%	1.75
Fold-4	97.79%	0.93
Fold-5	98.61%	0.74
Average	98.2%	1.12

Table 8 shows the confusion metrics for our model on test images. This is an error matrix [50] that allows visualisation of the performance. Each row of this matrix represents the instances in the predicted class, and each column represents the instances in ground truth. It becomes easy to see whether the model is confusing two classes and how significant the confusion is. An illustration is also shown in Figure 11 in percentage for the confusion metrics.

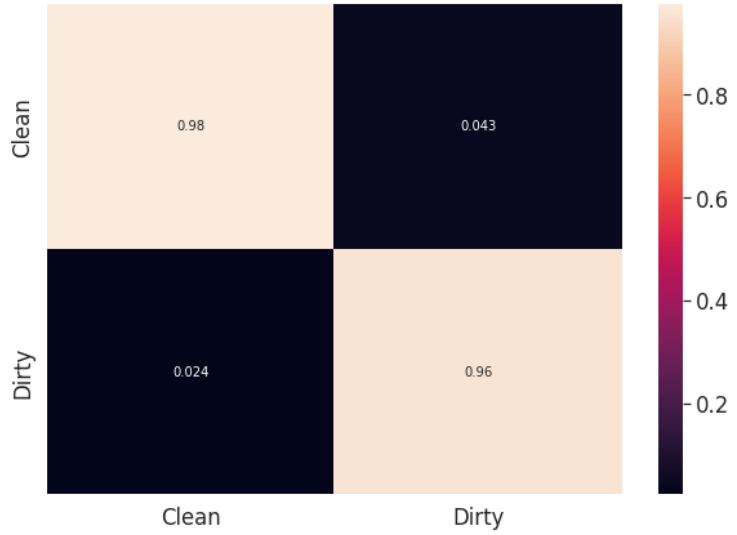

Figure 11. Confusion metrics in percentage where columns represents ground truth and rows represents predicted class.

It clearly shows very few images are mistaken to be in the wrong class. These are also known as false positives. It again helps us to calculate the *precision* with Equation (6).

$$Precision = \frac{TruePositive}{TruePositive + FalsePositive} \tag{6}$$

Figure 12 contains some examples of false positive detections from our work. Visually, they are almost indistinguishable, which might contribute to the missing classification.

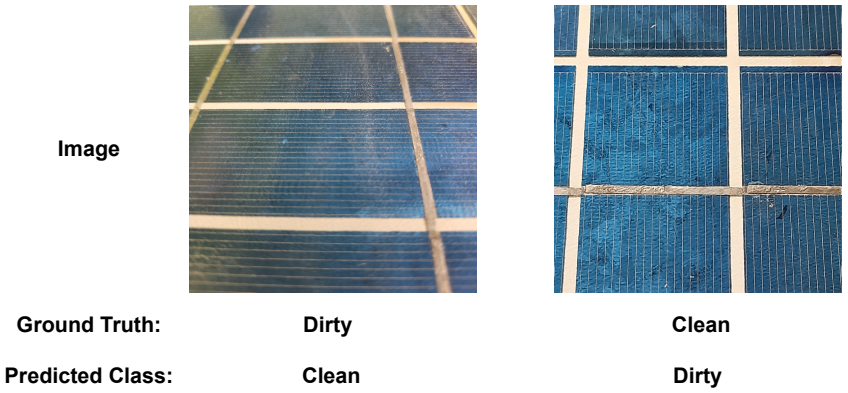

Figure 12. Examples of misclassification.

Table 8. Confusion metrics on test images.

		Ground-Truth Class	
		Clean	**Dirty**
Predicted class	Clean	412	18
	Dirty	10	400
Precision		97.6%	95.7%

In terms of accuracy, the proposed SolNet outperformed all the SOTA with a considerable margin in accuracy. Although the number of trainable parameters plays an important role in calculation speed, it is somewhat redundant for our problem statement.

Out of all the models, Resnet50 proposed by He et al. [46] performed poorly with over 60 millions trainable parameters. This suggests that using any residual information will not

correlate to an increase in accuracy. Again, even with two-fold more trainable parameters, Simonyan and Zisserman's [44] VGG16 architecture failed to obtain the highest accuracy because of model over-fitting. InceptionV3 proposed by Szegedy et al. [45] gave noticeable accuracy with only 6.4 M parameters. A comparison of accuracy and trainable parameters is shown in Table 9.

Table 9. Comparison of average testing accuracy for SOTA models and SolNet on our dataset.

Authors	Model	Accuracy	Trainable Parameters
Simonyan & Zisserman [44]	VGG16	97.5%	138M
Szegedy et al. [45]	InceptionV3	95.2%	6.4M
He et al. [46]	Resnet50	84.0%	60M
Krizhevsky et al. [47]	AlexNet	96.6%	62M
Proposed model	SolNet	98.2%	56M

5. Discussion

A good and balanced dataset is of prime concern for training a model. In this research, the pictures of the dataset were collected from different parts of Bangladesh with different dust patterns. The dataset performed similarly when trained with SOTA models, proving the viability of the dataset. Thus, this dataset can be used for further classification problems with machine learning and deep learning. Afterward, the proposed SolNet model was applied to the dataset. The model is a custom deep learning model where a higher accuracy of 98.2% was achieved with only 56 million parameters. Therefore, when the model was compared with the SOTA models, such as VGG16, Inception V3, AlexNet, and Resnet50, it produced better output in the mentioned parameters of evaluation. Moreover, it produced better results in comparison to similar work by other researchers on different datasets, such as the CNN LeNet model by Maity et al. [37] and the AlexNet model by Zyout et al. [38] that had an accuracy of 80% and 93.3%, respectively, on dust detection.

SolNet outperformed the mentioned models by a good margin of accuracy as shown in Table 7. It can also be seen that SolNet has a lower number of parameters than most of the prominent models which proves less complexity. Thus, the model was trained in less time with lower computational complexity. SolNet thus provided higher accuracy, lower training time, and less complexity. Although Google's InceptionV3 [45] still holds the lowest number of parameters and run-time, the accuracy is lower. As our application is not based on real-time feed, the trade-off between run-time and accuracy was dealt with accordingly.

However, model over-fit is a common barrier to producing robust models and testing the models with different variations of data is the way to detect it. Among different approaches available to overcome the over-fit problem, K-fold cross validation and early stopping were used in SolNet. For the cross validation, the dataset was divided into five folds of training sets and validation sets in such a way that the different patterns of the dataset could be trained and tested, and thus, the performance of the model could be evaluated for all variations of data in the dataset [51].

The five folds for cross validation are shown in Table 7. It shows that all the folds performed equally well, achieving higher than 96.46% accuracy with an average of 98.2%. Thus, it can be stated that the model performs adequately for a different train–test split of the dataset. Moreover, in Figure 10, the accuracy and loss graphs were plotted against epochs which shows the saturation of improvement in training to detect the point of early stopping. So, the values of loss and accuracy from this graph help decide that the training epochs should be 30. Other hyperparameters were similarly adjusted to make the model compatible for any unknown data without over-fitting or under-fitting as shown in Table 6.

6. Conclusions

The main aim of the SolNet architecture is to develop a CNN model that can detect the presence of dust on any solar panel. In this research, a dataset was introduced and images of the different levels of dust on the panels were collected from Bangladesh. Following the collection of 2231 images, manual sorting of the data was performed to classify 1130 images as clean and 1101 images as dirty. All the random-shaped original images were then reshaped to 227 × 227 × 3 sizes, keeping the features intact and made ready for the input to be fed to SolNet and other SOTA models of CNN. The dataset proved to be usable for further research as similar results were obtained in all the models. The dataset was then used in the proposed CNN model, SolNet. The proposed architecture comes with conv-pool pairs with three dense layers making 56M trainable parameters. This model ensures the reduction of computational complexity with a reduced number of trainable parameters. However, the usability of the model was proved as it provided an accuracy of 98.2% and a loss of 1.12 on average between 5 folds on the binary classification of images in 30 epochs. The cross validation of the model also proves its fitness of it for any unseen data.

Thus, SolNet outperformed the SOTA models in terms of our parameters of evaluation. The prospects of dust detection using CNN architecture are multi-dimensional. So, in the future, the SolNet model will be trained on datasets from different regions of the world. The enrichment of the dataset must be a prime concern to achieve the universality of the model. Moreover, the models from machine learning such as random forest, *k*-NN, XG boost, etc., can also be used to test the accuracy and performance of the aforesaid datasets. Lastly, the proposed CNN model can also be linked with some image processing functions if needed to make the model fit enough with any kind of unknown picture quality. In the future, extensive work can be undertaken to improve the dataset and introduce different classes for the type of dirt on the panels, such as dust, dust mixed with rain, water stains, and so on. The dataset can be enlarged with a greater collection of pictures from several parts of the world. Thus, models can be developed for multi-class classification. As SolNet is a custom CNN model, there is always the opportunity for fine-tuning it. Tweaking of hyperparameters, such as activation function and optimiser, can be employed to further improve the accuracy and reduce the loss and computational complexity.

Author Contributions: Conceptualization, M.S.H.O. and Z.M.M.S., methodology, M.S.H.O. and Z.M.M.S.; software, M.S.H.O. and A.A.; validation, M.S.H.O., A.A., A.K. and R.A.; writing—original draft preparation, A.K., S.T.H. and M.H.; writing—review and editing M.S.A., T.J., A.M.T.O. and A.K.A. All authors have read and agreed to the published version of the manuscript.

Funding: This research received no external funding.

Data Availability Statement: The data and implementation code are open-sourced for the researchers at the following link https://github.com/Onimee58/SolNET (accessed on 13 December 2022).

Acknowledgments: This study was an independent collaborative research work of all authors from four different institutions. The authors would like to express heartfelt thanks to their affiliated institutions Military Institute of Science and Technology, East-West University, Central Queensland University, Auckland University of Technology for supporting this research collaboration.

Conflicts of Interest: The authors declare no conflict of interest.

Abbreviations

The following abbreviations are used in this manuscript:

ANN	Artificial Neural Network
AE-LSTM	Auto-Encoder Long Short-Term Memory
CNN	Convolutional Neural Network
DBSI	Dry Bare Soil Index
FC	Fully Connected
GHG	Green House Gas
GEE	Google Earth Engine
HSV	Hue Saturation Value
IoT	Internet of Things
KNN	K Nearest Neighbor
PV	Photo Voltaic
SOTA	State Of The Art
VGG	Visual Geometry Group

References

1. Kabir, A.; Sunny, M.R.; Siddique, N.I. Assessment of grid-connected residential PV-battery systems in Sweden-A Techno-economic Perspective. In Proceedings of the 2021 IEEE International Conference in Power Engineering Application (ICPEA), Shah Alam, Malaysia, 8–9 March 2021; pp. 73–78.
2. IRENA. Renewable Capacity Statistics. 2022. Available online: https://www.irena.org/Publications/2022/Apr/Renewable-Capacity-Statistics-2022 (accessed on 23 August 2022).
3. Ritchie, H.; Roser, M.; Rosado, P. Renewable energy. Our World in Data. 2020. Available online: https://ourworldindata.org/renewable-energy (accessed on 24 August 2022).
4. Chanchangi, Y.N.; Ghosh, A.; Sundaram, S.; Mallick, T.K. Dust and PV Performance in Nigeria: A review. *Renew. Sustain. Energy Rev.* **2020**, *121*, 109704. [CrossRef]
5. Tanesab, J.; Parlevliet, D.; Whale, J.; Urmee, T. Dust effect and its economic analysis on PV modules deployed in a temperate climate zone. *Energy Procedia* **2016**, *100*, 65–68. [CrossRef]
6. Maghami, M.R.; Hizam, H.; Gomes, C.; Radzi, M.A.; Rezadad, M.I.; Hajighorbani, S. Power loss due to soiling on solar panel: A review. *Renew. Sustain. Energy Rev.* **2016**, *59*, 1307–1316. [CrossRef]
7. Santhakumari, M.; Sagar, N. A review of the environmental factors degrading the performance of silicon wafer-based photovoltaic modules: Failure detection methods and essential mitigation techniques. *Renew. Sustain. Energy Rev.* **2019**, *110*, 83–100. [CrossRef]
8. Kabir, M.A.; Islam, R.; Nazifa, S.; Choudhury, R. Dust Effect on Photovoltaic Output Performance: Comparative Analysis and A Case Study in Dhaka, Bangladesh. In Proceedings of the 2021 International Conference on Automation, Control and Mechatronics for Industry 4.0 (ACMI), Rajshahi, Bangladesh, 8–9 July 2021; pp. 1–6.
9. Dantas, G.M.; Mendes, O.L.C.; Maia, S.M.; de Alexandria, A.R. Detecção de poeira em painel solar usando técnicas de processamento de imagem: Uma revisão Dust detection in solar panel using image processing techniques: A review Detección de polvo en el panel solar utilizando técnicas de procesamiento por imágenes: Una revisión. *Res. Soc. Dev.* **2020**, *9*, e321985107.
10. Ghosh, A. Soiling losses: A barrier for India's energy security dependency from photovoltaic power. *Challenges* **2020**, *11*, 9. [CrossRef]
11. Ullah, A.; Imran, H.; Maqsood, Z.; Butt, N.Z. Investigation of optimal tilt angles and effects of soiling on PV energy production in Pakistan. *Renew. Energy* **2019**, *139*, 830–843. [CrossRef]
12. Paudyal, B.R.; Shakya, S.R. Dust accumulation effects on efficiency of solar PV modules for off grid purpose: A case study of Kathmandu. *Sol. Energy* **2016**, *135*, 103–110. [CrossRef]
13. Costa, S.C.; Diniz, A.S.A.; Kazmerski, L.L. Solar energy dust and soiling R&D progress: Literature review update for 2016. *Renew. Sustain. Energy Rev.* **2018**, *82*, 2504–2536.
14. Kazem, H.A.; Chaichan, M.T.; Al-Waeli, A.H.; Sopian, K. A review of dust accumulation and cleaning methods for solar photovoltaic systems. *J. Clean. Prod.* **2020**, *276*, 123187. [CrossRef]
15. Ramli, M.A.; Prasetyono, E.; Wicaksana, R.W.; Windarko, N.A.; Sedraoui, K.; Al-Turki, Y.A. On the investigation of photovoltaic output power reduction due to dust accumulation and weather conditions. *Renew. Energy* **2016**, *99*, 836–844. [CrossRef]
16. Benghanem, M.; Almohammedi, A.; Khan, M.T.; Al-Masraqi, A. Effect of dust accumulation on the performance of photovoltaic panels in desert countries: A case study for Madinah, Saudi Arabia. *Int. J. Power Electron. Drive Syst.* **2018**, *9*, 1356. [CrossRef]
17. Gholami, A.; Khazaee, I.; Eslami, S.; Zandi, M.; Akrami, E. Experimental investigation of dust deposition effects on photo-voltaic output performance. *Sol. Energy* **2018**, *159*, 346–352. [CrossRef]
18. Kazem, H.A.; Chaichan, M.T. Experimental analysis of the effect of dust's physical properties on photovoltaic modules in Northern Oman. *Sol. Energy* **2016**, *139*, 68–80. [CrossRef]
19. Chaudhary, A.; Chaturvedi, D. Thermal Image Analysis and Segmentation to Study Temperature Effects of Cement and Bird Deposition on Surface of Solar Panels. *Int. J. Image, Graph. Signal Process.* **2017**, *9*, 12–22. [CrossRef]

20. Phoolwani, U.K.; Sharma, T.; Singh, A.; Gawre, S.K. IoT Based Solar Panel Analysis using Thermal Imaging. In Proceedings of the 2020 IEEE International Students' Conference on Electrical,Electronics and Computer Science (SCEECS), Bhopal, India, 22–23 February 2020; pp. 1–5. [CrossRef]
21. Cubukcu, M.; Akanalci, A. Real-time inspection and determination methods of faults on photovoltaic power systems by thermal imaging in Turkey. *Renew. Energy* **2020**, *147*, 1231–1238. [CrossRef]
22. Thomas, S.K.; Joseph, S.; Sarrop, T.; Haris, S.B.; Roopak, R. Solar Panel Automated Cleaning (SPAC) System. In Proceedings of the 2018 International Conference on Emerging Trends and Innovations In Engineering And Technological Research (ICETIETR), Ernakulam, India, 11–13 July 2018; pp. 1–3. [CrossRef]
23. Zainuddin, N.F.; Mohammed, M.N.; Al-Zubaidi, S.; Khogali, S.I. Design and Development of Smart Self-Cleaning Solar Panel System. In Proceedings of the 2019 IEEE International Conference on Automatic Control and Intelligent Systems (I2CACIS), Selangor, Malaysia, 29 June 2019; pp. 40–43. [CrossRef]
24. Mohammed, H.A.; Al-Hilli, B.A.M.; Al-Mejibli, I.S. Smart system for dust detecting and removing from solar cells. *J. Physics: Conf. Ser.* **2018**, *1032*, 012055. [CrossRef]
25. Santosh Kumar, S.; shankar, S.; Murthy, K. Solar Powered PV Panel Cleaning Robot. In Proceedings of the 2020 International Conference on Recent Trends on Electronics, Information, Communication & Technology (RTEICT), Bangalore, India, 12–13 November 2020; pp. 169–172. [CrossRef]
26. Minh, H.V.T.; Avtar, R.; Mohan, G.; Misra, P.; Kurasaki, M. Monitoring and mapping of rice cropping pattern in flooding area in the Vietnamese Mekong delta using Sentinel-1A data: A case of an Giang province. *ISPRS Int. J. Geo-Inf.* **2019**, *8*, 211. [CrossRef]
27. Supe, H.; Avtar, R.; Singh, D.; Gupta, A.; Yunus, A.P.; Dou, J.; A Ravankar, A.; Mohan, G.; Chapagain, S.K.; Sharma, V.; et al. Google earth engine for the detection of soiling on photovoltaic solar panels in arid environments. *Remote Sens.* **2020**, *12*, 1466. [CrossRef]
28. Abuqaaud, K.A.; Ferrah, A. A novel technique for detecting and monitoring dust and soil on solar photovoltaic panel. In Proceedings of the 2020 Advances in Science and Engineering Technology International Conferences (ASET), Dubai, United Arab Emirates, 4 February–9 April 2020; pp. 1–6.
29. Tribak, H.; Zaz, Y. Dust Soiling Concentration Measurement on Solar Panels based on Image Entropy. In Proceedings of the 2019 7th International Renewable and Sustainable Energy Conference (IRSEC), Agadir, Morocco, 27–30 November 2019; pp. 1–4.
30. Sunny, M.R.; Kabir, M.A.; Naheen, I.T.; Ahad, M.T. Residential energy management: A machine learning perspective. In Proceedings of the 2020 IEEE Green Technologies Conference (GreenTech), Oklahoma City, OK, USA, 1–3 April 2020; pp. 229–234.
31. Igathinathane, C.; Melin, S.; Sokhansanj, S.; Bi, X.; Lim, C.; Pordesimo, L.; Columbus, E. Machine vision based particle size and size distribution determination of airborne dust particles of wood and bark pellets. *Powder Technol.* **2009**, *196*, 202–212. [CrossRef]
32. Maitre, J.; Bouchard, K.; Bédard, L.P. Mineral grains recognition using computer vision and machine learning. *Comput. Geosci.* **2019**, *130*, 84–93. [CrossRef]
33. Proietti, A.; Panella, M.; Leccese, F.; Svezia, E. Dust detection and analysis in museum environment based on pattern recognition. *Measurement* **2015**, *66*, 62–72. [CrossRef]
34. Saquib, D.; Nasser, M.N.; Ramaswamy, S. Image Processing Based Dust Detection and prediction of Power using ANN in PV systems. In Proceedings of the 2020 Third International Conference on Smart Systems and Inventive Technology (ICSSIT), Tirunelveli, India, 20–22 August 2020; pp. 1286–1292. [CrossRef]
35. Mehta, S.; Azad, A.P.; Chemmengath, S.A.; Raykar, V.; Kalyanaraman, S. Deepsolareye: Power loss prediction and weakly supervised soiling localization via fully convolutional networks for solar panels. In Proceedings of the 2018 IEEE Winter Conference on Applications of Computer Vision (WACV), Lake Tahoe, NV, USA, 12–15 March 2018; pp. 333–342.
36. Fan, S.; Wang, Y.; Cao, S.; Zhao, B.; Sun, T.; Liu, P. A deep residual neural network identification method for uneven dust accumulation on photovoltaic (PV) panels. *Energy* **2022**, *239*, 122302. [CrossRef]
37. Maity, R.; Shamaun Alam, M.; Pati, A. An Approach for Detection of Dust on Solar Panels Using CNN from RGB Dust Image to Predict Power Loss. In *Cognitive Computing in Human Cognition*; Springer: Berlin/Heidelberg, Germany, 2020; pp. 41–48.
38. Zyout, I.; Oatawneh, A. Detection of PV Solar Panel Surface Defects using Transfer Learning of the Deep Convolutional Neural Networks. In Proceedings of the 2020 Advances in Science and Engineering Technology International Conferences (ASET), Dubai, United Arab Emirates, 4 February–9 April 2020; pp. 1–4. [CrossRef]
39. Alimi, O.A.; Meyer, E.L.; Olayiwola, O.I. Solar Photovoltaic Modules' Performance Reliability and Degradation Analysis—A Review. *Energies* **2022**, *15*, 5964. [CrossRef]
40. Khilar, R.; Suba, G.M.; Kumar, T.S.; Samson Isaac, J.; Shinde, S.K.; Ramya, S.; Prabhu, V.; Erko, K.G. Improving the Efficiency of Photovoltaic Panels Using Machine Learning Approach. *Int. J. Photoenergy* **2022**, 1–6. [CrossRef]
41. Almalki, F.A.; Albraikan, A.A.; Soufiene, B.O.; Ali, O. Utilizing Artificial Intelligence and Lotus Effect in an Emerging Intelligent Drone for Persevering Solar Panel Efficiency. *Wirel. Commun. Mob. Comput.* **2022**, 1–12. [CrossRef]
42. Ibrahim, M.; Alsheikh, A.; Awaysheh, F.M.; Alshehri, M.D. Machine learning schemes for anomaly detection in solar power plants. *Energies* **2022**, *15*, 1082. [CrossRef]
43. Yousif, J.H.; Kazem, H.A.; Al-Balushi, H.; Abuhmaidan, K.; Al-Badi, R. Artificial Neural Network Modelling and Experimental Evaluation of Dust and Thermal Energy Impact on Monocrystalline and Polycrystalline Photovoltaic Modules. *Energies* **2022**, *15*, 4138. [CrossRef]
44. Simonyan, K.; Zisserman, A. Very Deep Convolutional Networks for Large-Scale Image Recognition. *arXiv* **2014**, arXiv:1409.1556.

45. Szegedy, C.; Vanhoucke, V.; Ioffe, S.; Shlens, J.; Wojna, Z. Rethinking the Inception Architecture for Computer Vision. In Proceedings of the 2016 IEEE Conference on Computer Vision and Pattern Recognition (CVPR), Las Vegas, NV, USA, 27–30 June 2016; pp. 2818–2826.
46. He, K.; Zhang, X.; Ren, S.; Sun, J. Deep Residual Learning for Image Recognition. In Proceedings of the 2016 IEEE Conference on Computer Vision and Pattern Recognition (CVPR), Las Vegas, NV, USA, 27–30 June 2016; pp. 770–778.
47. Krizhevsky, A.; Sutskever, I.; Hinton, G.E. ImageNet Classification with Deep Convolutional Neural Networks. In *Advances in Neural Information Processing Systems*; Pereira, F., Burges, C., Bottou, L., Weinberger, K., Eds.; Curran Associates, Inc.: New York, NY, USA, 2012; Volume 25.
48. Russakovsky, O.; Deng, J.; Su, H.; Krause, J.; Satheesh, S.; Ma, S.; Huang, Z.; Karpathy, A.; Khosla, A.; Bernstein, M.; et al. ImageNet Large Scale Visual Recognition Challenge. *Int. J. Comput. Vis.* **2015**, *115*, 211–252. . [CrossRef]
49. Onim, M.S.H.; Nyeem, H.; Roy, K.; Hasan, M.; Ishmam, A.; Akif, M.A.H.; Ovi, T.B. BLPnet: A new DNN model and Bengali OCR engine for Automatic Licence Plate Recognition. *Array* **2022**, *15*, 100244. [CrossRef]
50. Stehman, S.V. Selecting and interpreting measures of thematic classification accuracy. *Remote Sens. Environ.* **1997**, *62*, 77–89. . [CrossRef]
51. Bergmeir, C.; Hyndman, R.J.; Koo, B. A note on the validity of cross-validation for evaluating autoregressive time series prediction. *Comput. Stat. Data Anal.* **2018**, *120*, 70–83. [CrossRef]

Disclaimer/Publisher's Note: The statements, opinions and data contained in all publications are solely those of the individual author(s) and contributor(s) and not of MDPI and/or the editor(s). MDPI and/or the editor(s) disclaim responsibility for any injury to people or property resulting from any ideas, methods, instructions or products referred to in the content.